Quantum Electronics **48** (12) 1118–1127 (2018)

https://doi.org/10.1070/QEL16845

Possibilities of laser amplification and measurement of the field structure of ultrashort pulses in the range of 2.7–3 μm in tellurite glass fibres doped with erbium ions

E.A. Anashkina, V.V. Dorofeev, S.V. Muravyev, S.E. Motorin, A.V. Andrianov, A.A. Sorokin, M.Yu. Koptev, S. Singh, A.V. Kim

Abstract. **The amplification of ultrashort signals in the range 2.7–3 μm in active tellurite glass fibres with high Kerr nonlinearity and high concentration of erbium ions in the core is theoretically investigated under diode pumping at a wavelength of 0.975 μm. The possibility of producing pulses with the energy ~10 nJ and the duration smaller than 100 fs with ~20 dB gain is shown. Moreover, using a specially developed iterative computer algorithm, the possibility of determining the intensity and phase of the generated pulses by measuring their fundamental spectra and two additional spectra obtained by means of nonlinear-optical conversion in short pieces of these optical fibres is demonstrated. Optical fibre samples are made of high-purity $TeO_2–ZnO–La_2O_3–Na_2O$ glasses with 10^{21} cm^{-3} concentration of erbium ions in the core and a low content of hydroxyl groups that causes small losses in the spectral range under consideration. The group velocity dispersions, effective mode fields, nonlinear coefficients and field overlap integrals of the LP_{01} fundamental modes with a doped core for optical fibres with different core diameters are calculated, and the emission and absorption cross sections are calculated basing on the experimental luminescence spectrum. The optimal parameters of the amplifier are determined by numerically modelling the dynamics of ultrashort pulses using the measured and calculated characteristics.**

Keywords: *tellurite glass optical fibre, erbium ions, laser amplifier simulation, ultrashort pulse phase measurement.*

E.A. Anashkina Institute of Applied Physics, Russian Academy of Sciences, ul. Ul'yanova 46, 603950 Nizhny Novgorod, Russia; Lobachevsky State University of Nizhny Novgorod, prosp. Gagarina 23, 603950 Nizhny Novgorod, Russia; Center of Laser Technology and Materials Science, ul. Vavilova 38, korp. L-2, 119991 Moscow, Russia; e-mail: elena.anashkina@gmail.com;
V.V. Dorofeev, S.E. Motorin Center of Laser Technology and Materials Science, ul. Vavilova 38, korp. L-2, 119991 Moscow, Russia; G.G. Devyatykh Institute of Chemistry of High-Purity Substances, Russian Academy of Sciences, ul. Tropinina 49, 603950 Nizhny Novgorod, Russia;
S.V. Muravyev, A.A. Sorokin Institute of Applied Physics, Russian Academy of Sciences, ul. Ul'yanova 46, 603950 Nizhny Novgorod, Russia; Lobachevsky State University of Nizhny Novgorod, prosp. Gagarina 23, 603950 Nizhny Novgorod, Russia;
A.V. Andrianov, M.Yu. Koptev, A.V. Kim Institute of Applied Physics, Russian Academy of Sciences, ul. Ul'yanova 46, 603950 Nizhny Novgorod, Russia;
S. Singh Sant Longowal Institute of Engineering & Technology, Longowal, Sangrur, Punjab, India-148106

Received 9 October 2018; revision received 14 October 2018
Kvantovaya Elektronika **48** (12) 1118–1127 (2018)
Translated by V.L. Derbov

1. Introduction

The development of new methods and approaches for generating laser radiation in the wavelength range above 2 μm is an important problem, since the sources of such radiation are of interest for many applications, including noninvasive medical diagnostics, laser surgery, space research, wireless optical communications, gas composition detection, and remote detection of organic compounds (including biomarkers), explosives and toxic substances [1]. Various types of coherent optical sources of the mid-IR range are experimentally demonstrated and theoretically investigated, including both direct laser generators and systems based on signal conversion in nonlinear optical elements (see, e.g., [1–12]). A promising direction of study is the development of fibre systems that have good weight and size specifications, high quality of the laser beam and high-efficiency heat sink. Silica fibres traditionally used for telecommunications at a wavelength of 1.55 μm have large losses in the spectral region above 2.2 μm, which limits their use. Optical fibres based on chalcogenide, tellurite and fluoride glasses may have suitable parameters for operating in the mid-IR range [13].

Tellurite glasses are transparent in the near-IR and mid-IR ranges (up to 5–6 μm), have high chemical resistance, high nonlinear refractive index (10–20 times greater than that of fused silica), allow the possibility of doping with rare earth ions with high concentrations, and are resistant to crystallisation (for many compositions) [12–25]. Erbium-doped fibres from tellurite glass appear promising laser media for the 2.7–3 μm range due to lasing and gain at the transition $^4I_{11/2} \rightarrow {}^4I_{13/2}$ under diode pumping at a wavelength of 0.975 μm (transition $^4I_{15/2} \rightarrow {}^4I_{11/2}$) (Fig. 1). However, despite the marked advantages of tellurite glasses, their use requires the solution of a number of problems. In particular, it is necessary to develop the technology of deep dehydration of glasses to minimise absorption in the range of 2.7–3 μm. In addition, because of the relatively high phonon energy, the lifetime τ_3 of the upper laser level $I_{11/2}$ is by an order of magnitude shorter than the lifetime τ_2 of the lower-lying laser level $^4I_{13/2}$, which makes it difficult to provide a population inversion between them [17, 19]. Therefore, for efficient depopulation of the $^4I_{13/2}$ level, various options and schemes are offered, including two-colour cascade generation [3], generation with pump pulses having the duration $\sim\tau_3$ and the repetition rate $\sim 1/\tau_2$ (so that the population of the metastable level $^4I_{13/2}$ could relax before the next pumping pulse arrival) [19], as well as the use of very high concentrations of erbium, at which the

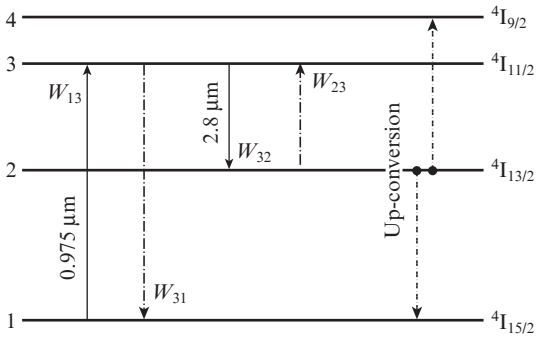

Figure 1. Simplified diagram of erbium ion energy levels.

rate of two-photon up-conversion process ($^4I_{13/2}$ + $^4I_{13/2}$ → $^4I_{9/2}$ + $^4I_{15/2}$) is high [17].

This paper explores the last option. We developed and manufactured an optical fibre from high-purity glass TeO_2–ZnO–La_2O_3–Na_2O with an erbium-doped core with the concentration of active ions of 10^{21} cm^{-3} and with low content of hydroxyl groups that provides low losses in the spectral range under consideration. Previously we reported on the fabrication of a fibre with erbium-doped core based on TeO_2–WO_3–La_2O_3–Bi_2O_3 glass, for which the time τ_3 was ~100 μs [19]. Due to the lower phonon energy, in zinc-tellurite glasses the lifetime τ_3 is longer than in tungstate-tellurite glasses [13, 17]. In addition, for zinc-tellurite glasses, the maximum of the absorption peak caused by hydroxyl groups (~3.3 μm) [21, 22] is shifted to a longer wavelength region relative to the peak for tungstate-tellurite glasses, which is located at a wavelength of ~3.3 μm [20, 22]. This can reduce the absorption and quenching of erbium ions luminescence by hydroxyl groups in TeO_2–ZnO–La_2O_3–Na_2O fibres in the range of 2.7–3 μm.

In this paper, we consider the possibility of producing a source of ultrashort pulses with ~10 nJ energy in 2.7–3 μm spectral range, using amplification of seed signals with ~100 pJ energy in the fabricated high-purity tellurite glass optical fibres with high Kerr nonlinearity and high concentration of erbium ions in the core. The seed signals can be obtained, e.g., using the Raman frequency shift of optical solitons in germanate optical fibres [26]. As far as we know, the amplification of ultrashort pulses at the transition $^4I_{11/2}$ → $^4I_{13/2}$ in erbium-doped tellurite glass fibres has not been previously studied, although the luminescence with a linewidth of more than 200 nm has been observed by a few research teams [17–19].

Measurement of the field structure of the ultrashort pulses in the spectral range studied by us is undoubtedly relevant. The methods of autocorrelation function and frequency-resolved optical gating (FROG), based on the second harmonic generation in a nonlinear crystal and traditionally used in the near-infrared region for fibre laser systems, have a number of disadvantages, including ambiguity in the choice of the time axis direction and phase sign, as well as the restriction on the spectral width of the measured signals due to the finite width of the phase matching in the crystal [27]. Adaptation of these methods for the range 2.7–3 μm is additionally associated with the difficulty of choosing optical elements. In addition, registration of the second harmonic spectra is impossible using standard silicon photodetectors (with a sensitivity limit of up to ~1.1 μm); therefore, it is necessary to use detectors that are more expensive. Recently, a simple method free of these drawbacks has been proposed and demonstrated experimentally for measuring waveforms with a minimum set of used optical elements [28]. The method is based on recording the fundamental spectrum (spectrum of the original signal) and two additional spectra obtained as a result of radiation conversion in media with cubic optical nonlinearity: in glasses or polymer films in the case of high-power laser systems [28, 29] or in non-linear optical fibre segments in the case of fibre systems [30, 31]. Using a specially developed iterative computer algorithm, three spectral measurements are processed, allowing reconstruction of the wave electric field structure, i.e., the intensity and phase distribution. In the present work, we also numerically demonstrate the possibility of successful application of this method for measuring amplified pulses directly in an active tellurite glass fibre without using additional optical elements.

2. Fabrication of tellurite glasses and active optical fibres based on them

Glasses having the compositions TeO_2–ZnO–La_2O_3–Na_2O–Er_2O_3 (core, TZLNEr, Er^{3+} erbium ion concentration 1.06×10^{21} cm^{-3}) and TeO_2–ZnO–La_2O_3–Na_2O (claddings, TZLN-1 and TZLN-2) were synthesised by melting in platinum crucibles inside a sealed reactor made of silica glass in an atmosphere of purified oxygen [22].

For the preparation of the batch, initial reagents of special purity were used: tellurium dioxide TeO_2, purified by vacuum distillation according to a patented procedure; zinc oxide ZnO obtained by oxidising dimethyl zinc vapour in an oxygen-hydrogen burner flame [23]; commercially available lanthanum oxide La_2O_3; erbium oxide Er_2O_3; and sodium bicarbonate Na_2CO_3 of ACS purity grade. The total (weight) content of impurities, the most harmful in the visible and near-IR regions transition 3d-metals, in the mixture of initial reagents did not exceed 0.2–2 ppm, and the total concentration of rare-earth elements was less than 1–2 ppm [24]. Previous studies have shown that the melting technique used does not lead to significant contamination of the glass mass by optically active impurities during synthesis in platinum crucibles (except the platinum impurity) [25].

A monolithic two-layer preform and a jacketing tube for producing multimode and single-mode optical fibres with a step refractive index profile with an erbium-doped core were made using the technique applied to tungstate–tellurite glasses in [19]. In two-layer castings, the 'dry' core is protected from external influence by the cladding at all stages of the formation of optical fibre. The ends of the castings were mechanically ground and polished. After cutting and polishing, the preform had the following dimensions: outer diameter 14 mm, core diameter 3–4 mm, and length 44 mm. Photographs of the preform and the jacketing tube are shown in Fig. 2.

The transmission spectra in the IR range were recorded using the Nicolet 6700 IR Fourier spectrometer. The transmission spectra of both the entire preform 4.4 cm long and its segment 0.23 cm long were studied (Fig. 3a). The transparency region of zinc-tellurite glass doped with erbium ions extends to a wavelength of ~6 μm, and the absorption band of erbium with a maximum of ~1.55 μm is present in the spectra of both samples. Due to the use of the original method of melt dehydration, the absorption bands of hydroxyl groups with peaks at ~3.3 and ~4.4 μm and the overtone line with a

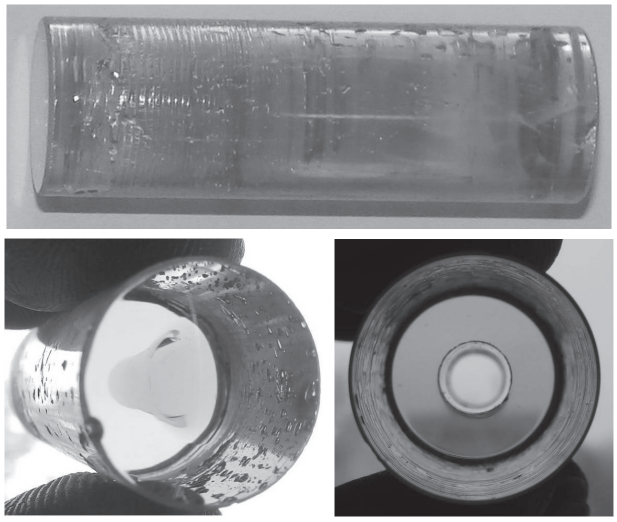

Figure 2. Photos of the preform and jacketing tube.

maximum at ~2.3 μm typical for ordinary tellurite glass samples are practically imperceptible in the spectrum of a thin sample. At the same time, the broad main absorption band of hydroxyl with a maximum of about 3.3 μm is clearly visible in the transmission spectrum of the entire preform, and there are no absorption bands of 2.3 and 4.4 μm, which indicates a low content of hydroxyl groups. In this case, a sharp decrease in the transmission after a wavelength of 4 μm is observed, which is explained by multiphonon absorption and, possibly,

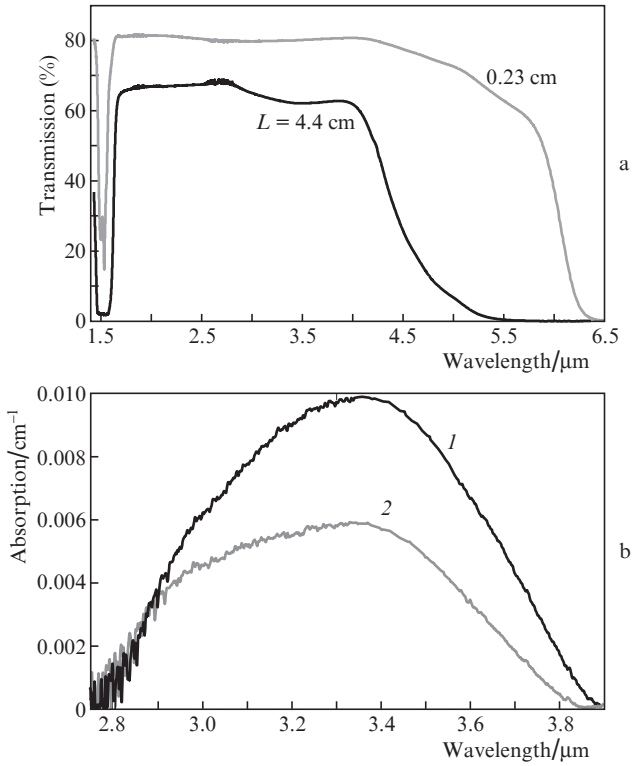

Figure 3. (a) Transmission spectra of the preform core with the length L = 4.4 and 0.23 cm and (b) absorption spectra in the region of the fundamental band of the hydroxyl group for (*1*) the core and (*2*) the cladding of the preform.

by the influence of the hydroxyl group absorption band with a maximum at ~4.4 μm. The study of the transmission spectra of sufficiently long samples of high-purity zinc-tellurite glass shows that the region of small losses and, therefore, efficient use of such glass for continuous fibre-optic devices is limited to a wavelength of ~4.4 μm.

When calculating the volume coefficient of absorption by hydroxyl in a piece of tellurite glass of sufficient length (more than 1 cm), it is possible to neglect the absorption at the ends, which for tellurite glass is usually several thousandths of a cm^{-1} [22]. As in Ref. [19], the spectra of the volume coefficient of absorption by hydroxyl groups were calculated for core glass and the cladding of the preform 4.4 cm long using the measured transmission spectra and the Bouguer–Lambert–Beer law (Fig. 3,b). The applied method of manufacturing preforms allows obtaining a low concentration of hydroxyl groups (~10^{-17} cm^{-3}), corresponding to an absorption coefficient of ~0.01 cm^{-1} in the band maximum near 3.3 μm for the core and ~0.006 cm^{-1} for the preform cladding (Fig. 3b).

By jacketing, the single-mode optical fibres with a polymeric protective coating were made. By changing the drawing speed, we obtained samples of fibres with different diameters of the TZLNEr glass core, the first TZLN-1 glass cladding, and the second TZLN-2 glass cladding.

3. Experimental measurement of the luminescence spectra, calculation of emission and absorption cross sections and shape of the gain band at the transition $^4I_{11/2} \rightarrow {}^4I_{13/2}$

To measure the luminescence spectra at the $^4I_{11/2} \rightarrow {}^4I_{13/2}$ transition in the manufactured tellurite glass fibres, a sample 5 cm long was pumped into the core with a diameter of 10 μm by radiation of a single-mode laser diode at a wavelength of 974 nm (3S Photonics, 400 mW). The image of the fibre end (the core and the first cladding) obtained with a microscope is shown in the inset in Fig. 4a. The diode radiation was coupled into the active fibre using two lenses. From the fibre output the radiation was directed to a Solar TII, MS2004I spectrometer with an InSb-based IR-detector (Infrared Associates) cooled with liquid nitrogen. The signal from the detector was fed into an amplifier and a lock-in signal amplifier. The measured signal was processed by a computer. The experimentally measured luminescence spectrum is shown in Fig. 4a.

Using the obtained luminescence spectrum, the emission cross section σ_{32} was calculated using the Füchtbauer–Ladenburg formula [32]; the absorption cross section σ_{23} was calculated using the McCumber method [33]. The results of the calculations are presented in Fig. 4b.

Knowing both cross sections of the $^4I_{11/2} \rightarrow {}^4I_{13/2}$transition, we calculated the shape of the gain band. It is known that the gain is proportional to the function

$$G = \sigma_{32}N_3 - \sigma_{23}N_2 = N_2(\sigma_{32}N_3/N_2 - \sigma_{23}), \quad (1)$$

where N_2, N_3 are the populations of the levels $^4I_{11/2}$ and $^4I_{13/2}$, respectively. Since the gain function $\sigma_{32}N_3/N_2 - \sigma_{23}$, shown in Fig. 4c, should be positive, the gain can be achieved at the long-wavelength wing (relative to the maximum of the emission cross section) even if $N_3 < N_2$.

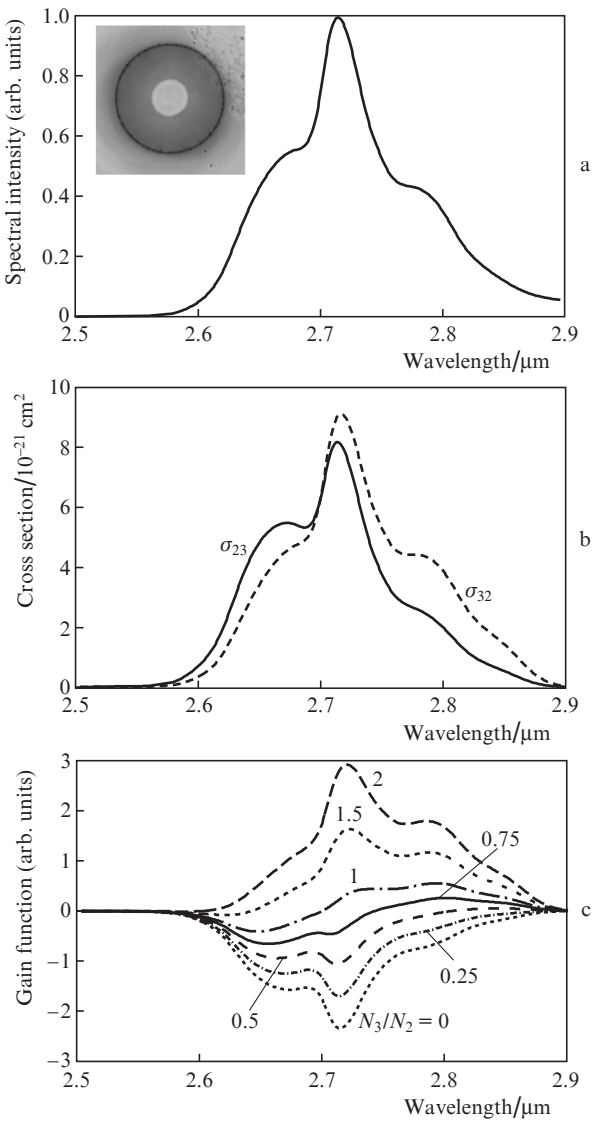

Figure 4. (a) Experimentally measured luminescence spectrum at the transition $^4I_{11/2} \rightarrow {}^4I_{13/2}$, (b) the emission and absorption cross sections calculated on its basis, and (c) the function characterising the shape of the gain band for different ratios of populations N_3/N_2 of the levels $^4I_{11/2}$ and $^4I_{13/2}$. The inset shows an image of the fibre end (the core and the first cladding).

4. Calculation of the dispersion and nonlinear characteristics of tellurite glass optical fibres

To find the propagation constants $\beta(\omega)$ and transverse structures of the electric field $F(r,\omega)$ of the fundamental modes LP_{01} of axially symmetric optical fibres made from tellurite glass with different diameters of the doped cores, the eigenvalue problem for the Helmholtz equation was solved. The mathematical formulation of the problem has the following form [34]:

$$\frac{d^2F}{dr^2} + \frac{1}{r}\frac{dF}{dr} + n^2(r,\omega)\frac{\omega^2}{c^2}F - \beta^2 F = 0, \tag{2}$$

$$F(r \rightarrow \infty) \rightarrow 0, \tag{3}$$

$$\frac{dF}{dr}(r = 0) = 0, \tag{4}$$

where r is the radial coordinate; n is the refractive index; c is the speed of light; $\omega = 2\pi c/\lambda$ is the angular frequency; and λ is the wavelength. The refractive index n_{clad} of the cladding glass was calculated using the Sellmeier formula,

$$n^2_{clad}(\lambda) = C_1 + \frac{C_2}{1 - C_3/\lambda^2} + \frac{C_4}{1 - C_5/\lambda^2}, \tag{5}$$

with the coefficients $C_1 = 2.18$, $C_2 = 1.617$, $C_3 = 0.45$ μm^2, $C_4 = 2.476$, and $C_5 = 225$ μm^2, the core refractive index being $n_{core} = 1.0045 n_{clad}$.

The normalisation of the function $F(r,\omega)$ was chosen as

$$\int_0^\infty |F(r,\omega)|^2 dr = 1. \tag{6}$$

To find the eigenvalues and eigenfunctions of the Helmholtz equation, a finite-difference scheme was used.

Figure 5 shows the calculated values of the group velocity dispersion $\beta_2 = \partial^2\beta/\partial\omega^2$ and nonlinear coefficients

$$\gamma = \frac{n_2\omega}{cA_{eff}} \tag{7}$$

for optical fibres of various diameters. Here, $n_2 = 3.8 \times 10^{-19}$ m^2 W^{-1} is the nonlinear refractive index of tellurite glass [15]; and

$$A_{eff} = \frac{\left[\int_0^\infty |F(r,\omega)|^2 2\pi r dr\right]^2}{\int_0^\infty |F(r,\omega)|^4 2\pi r dr} \tag{8}$$

is the effective mode area [35].

For cores of larger diameter, the contribution of the waveguide component of the dispersion is small, and the disper-

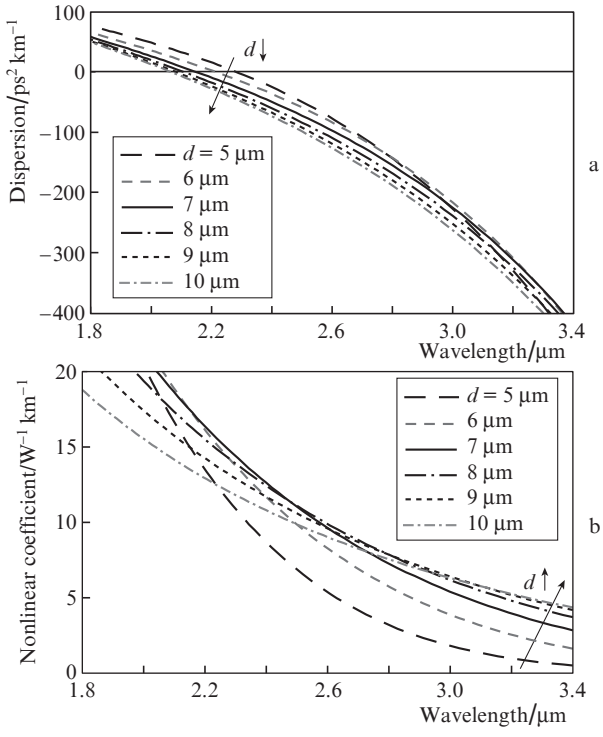

Figure 5. Calculated (a) group velocity dispersion β_2 and (b) nonlinear coefficients γ for optical fibres with different core diameters d.

sion zero is located near zero of the material dispersion (~2.04 μm). With decreasing diameter, the zero position begins to shift to the long-wavelength region. The decrease in the nonlinear coefficient γ with increasing wavelength is explained by both a decrease in the frequency ω in Eqn (7) and an increase in the effective area of the mode. The overlap integrals Γ_{32} of the LP_{01} fundamental mode field at a wavelength of 2.8 μm with a doped core are 0.05, 0.2, 0.36, 0.5, 0.61, 0.7, 0.76, 0.8 and 0.84 for diameters d = 4, 5, 6, 7, 8, 9, 10, 11, and 12 μm, respectively. For small d, the value of the parameter V is small (V = 0.82 for d = 4 μm), and so the mode is weakly localised near the core [35], and for relatively large values of d, the fibre ceases to be single-mode. The cut-off wavelength λ_{cutoff} = 2.8 μm is achieved with a diameter of ~12 μm.

5. Numerical simulation of the amplification of ultrashort pulses

To study the amplification of ultrashort pulses numerically, we used a model comprising rate equations for level populations N_1, N_2, N_3 normalised to the concentration of erbium ions N_{Er} (see Fig. 1), as well as an equation describing the variation of the pump power P_{31} along the fibre. The generalised nonlinear Schrödinger equation for the complex amplitude of the field $E(z,t)$ of an ultrashort pulse allowed for dispersion, Kerr and Raman nonlinearities of the fibre, linear losses $\alpha(\omega)$ and stimulated amplification and absorption at the transition $^4I_{11/2} \rightarrow {}^4I_{13/2}$. We assumed that the pump and signal propagate in the same direction. We took into account the two-photon up-conversion process ($^4I_{13/2} + {}^4I_{13/2} \rightarrow {}^4I_{9/2} + {}^4I_{15/2}$), absorption by hydroxyl groups, and multi-phonon absorption. The population of the $^4I_{9/2}$ level was neglected because of its short lifetime [17]. A quasi-stationary pulse amplification regime with a repetition rate of ν = 1 MHz under the action of continuous pumping at the $^4I_{15/2} \rightarrow {}^4I_{11/2}$ transition with a wavelength of λ_{31} = 0.975 μm was considered. The system of rate equations has the form [17]:

$$\frac{\partial N_1}{\partial t} = -W_{13}N_1 + \frac{1}{\tau_2}N_2 + \left(W_{31} + \frac{\eta_{31}}{\tau_3^R}\right)N_3 + K_{ETU}N_2^2 = 0, \quad (9)$$

$$\frac{\partial N_2}{\partial t} = -\left(W_{23} + \frac{1}{\tau_2}\right)N_2 - 2K_{ETU}N_2^2 + \left(W_{32} + W_{OH} + W_{mp} + \frac{\eta_{32}}{\tau_3^R}\right)N_3 = 0, \quad (10)$$

$$N_1 + N_2 + N_3 = 1, \quad (11)$$

Here, η_{31} = 0.84 and η_{32} = 0.16 are the luminescence branching ratios [17]; K_{ETU} = 3800 s^{-1} is the up-conversion ratio [17]; τ_3^R = 2.8 ms is the radiative lifetime of the $^4I_{11/2}$ level [17]; τ_2 is the total lifetime of the $^4I_{13/2}$ level, W_{OH} is the rate of absorption by hydroxyl groups; W_{mp} is the multiphonon absorption rate (the total lifetime τ_3 = 300 μs includes the radiative and nonradiative lifetimes: $1/\tau_3 = W_{OH} + W_{mp} + 1/\tau_3^R$ [17]);

$$W_{13,31} = \frac{\Gamma_{31}\lambda_{31}\sigma_{13,31}}{hcA_{core}}P_{31} \quad (12)$$

are the stimulated absorption and emission rates of the pump [2]; h is Planck's constant; A_{core} is the core cross-section area; Γ_{31} is the overlap integral of the transverse distribution of the pump field with the doped core; and $\sigma_{13} = 4 \times 10^{-21}$ cm^2 and $\sigma_{31} = 3 \times 10^{-21}$ cm^2 are the absorption and emission cross sections at the pump wavelength. The stimulated emission and absorption rates of the signal at the centre wavelength λ_{31} = 2.8 μm were set as [36]:

$$W_{32,23} = \frac{\Gamma_{32}\lambda_{32}}{hcA_{core}}\nu\int\sigma_{32,23}(\omega)\,|\tilde{E}(\omega)|^2 d\omega. \quad (13)$$

Here and below $\tilde{E}(z,\omega)$ is the Fourier transform of the function $E(z,t)$ defined via the Fourier transform operator $\hat{F}$:

$$\tilde{E}(z,\omega) = \hat{F}[E(z,t)]. \quad (14)$$

The equation describing the evolution of the pump power along the fibre was written in the following form [2, 37]:

$$\frac{dP_{31}}{dz} = -\Gamma_{31}N_{Er}(\sigma_{13}N_1 - \sigma_{31}N_3)P_{31} - \alpha_{31}P_{31}. \quad (15)$$

In the calculations, the experimentally measured background optical losses at the pump wavelength were used: α_{31} = 1 dB m^{-1}.

The generalised nonlinear Schrödinger equation for the complex amplitude of the ultrashort pulse field was written as [35, 36]

$$\frac{\partial\tilde{E}(z,\omega)}{\partial z} - i\gamma\hat{F}\left[E(z,t)\int R(t-\tau)\,|E(z,\tau)|^2 d\tau\right] + i\beta\tilde{E}(z,\omega) = \frac{g(\omega)-\alpha(\omega)}{2}\tilde{E}(z,\omega) \quad (16)$$

with the Raman response function $R(t-\tau)$, specified similar to that of Ref. [16], and with the gain function

$$g(\omega) = \Gamma_{32}N_{Er}(\sigma_{32}N_3 - \sigma_{23}N_2). \quad (17)$$

To solve Eqn (16), the split-step Fourier method (SSFM) [35] was applied using the fast Fourier transform (FFT) and inverse FFT (IFFT). The step along the fibre axis dz was chosen to be 10 μm. The evolution of the pump power was calculated in parallel. After each step in z, the values of the populations were found numerically, which were substituted into the corresponding equations at the next step. We have verified that reducing the step by two times does not change the calculation results.

When studying the gain of ultrashort optical signals in an active fibre, the input pulses chirped in a medium with anomalous dispersion were set to have an energy of 100 pJ and a duration of 600 fs. The duration of the soliton-shaped transform limited pulses was 300 fs (at half-maximum level). Such pulses can be formed, e.g., in nonlinear germanate fibres due to the tuning of the carrier wavelength of Raman solitons with their subsequent attenuation due to optical losses, after which the pulse ceases to be a soliton and its dispersive spreading occurs [26]. It was assumed that the pump radiation is coupled into the core and the overlap integral is Γ_{31} = 0.9 for all its diameters. In the numerical simulation, we used the dispersion dependences shown in Fig. 5a, and neglected the spectral dependence of the nonlinear coefficient γ and the overlap integral Γ_{32} for the pulses initially set at a central wavelength of 2.8 μm. The nonlinear coefficient γ was determined from the dependences shown in Fig. 5b, for each core diameter.

The values of Γ_{32} used in the calculations are given in the previous section. Since the mode field is weakly localised in a fibre with a thin core, fibres with a diameter of less than ~6 μm were not considered.

Figure 6a shows the calculated dependences of the pump power inside the fibre on z for different core diameters, and Fig. 6b shows the dependences of the energy of the amplified pulses ($\int|E(t)|^2 dt$) on the length of the active fibre. It can be seen that the smaller d, the greater the length of the pumped fibre segment, since the pump intensity increases at the same power. For the energy of the amplified signals, there is an optimum for the diameter of the core, since for small d the overlap integral Γ_{32} is small, and for relatively large d the pump length becomes smaller. At the optimal diameter (d = 7 μm, for which at a wavelength of 2.8 μm β_2 = –150 ps^2 km^{-1}, γ = 7.5 W^{-1} km^{-1}, Γ_{32} = 0.5), the maximum energy in the amplified pulse is ~10 nJ, i.e., a gain of ~20 dB is achieved (Fig. 6b).

Studies of the spectral and temporal dynamics of pulses in active silica fibres with anomalous dispersion showed that in such systems self-compression of pulses in the time domain can occur [38, 39]. Earlier, the amplification of a soliton pulse, whose carrier wavelength is gradually shifted beyond the gain band due to stimulated Raman scattering [40], was experimentally demonstrated and theoretically studied. In the case under consideration, a similar scenario of the nonlinear dynamics of the signal is implemented. At first, when the energy of the propagating pulse is low, the pulse duration increases due to the effect of dispersion and the shape of the spectrum changes only slightly. With increasing energy, the influence of nonlinearity begins to manifest itself and a noticeable spectral broadening occurs, due to self-phase modulation. The combined effect of the Kerr nonlinearity and anomalous dispersion leads to compression of the signal in the time domain (Fig. 6c). The duration of the thus compressed pulses is less than 100 fs (the minimum value is ~30 fs). The spectrum is broadened to such an extent that its short-wavelength wing falls in the region of normal dispersion and the dispersive waves are generated (the mechanism of their generation is described, e.g., in [35]). In the long-wavelength region of the spectrum, a soliton begins to form, the carrier wavelength of which gradually increases due to stimulated Raman scattering. Figure 7 shows the dependences of the square root of the spectral amplitude on the lengths of fibres of various diameters.

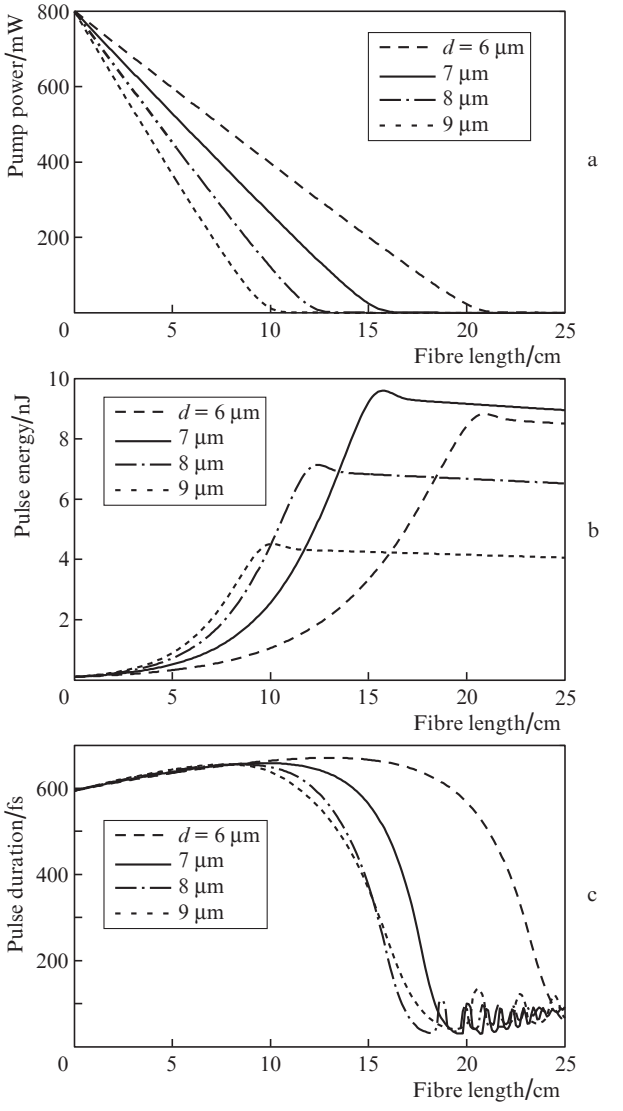

Figure 6. Dependences of (a) the pump power, (b) energy and (c) duration of amplified pulses, set at a centre wavelength of 2.8 μm, as a function of the length of active fibres with different core diameters d.

In the considered case of the amplification of seed pulses with 600 fs duration, the maximum energy of the amplified pulses is limited by the pump power. When using shorter seed pulses, the limiting factor can be nonlinear effects, which begin to significantly manifest themselves at lengths that are shorter than the pump absorption length. Indeed, during self-compression followed by the formation of a Raman soliton, its wavelength can go outside the gain band at a positive gain value (17), i.e., the soliton amplification stops earlier than in the case when its wavelength is not shifted due to the Raman effect.

6. Measurement of the field structure of ultrashort pulses

The method for determining the shape and phase of ultrashort pulses based on three spectral measurements proposed in Ref. [28] implies the application of an iterative algorithm to the fundamental (initial) spectrum $I_0(\Omega)$ and two spectra, $I_1(\Omega)$ and $I_2(\Omega)$, obtained by signal conversion in a dispersion-free medium with Kerr nonlinearity for the values of B-integrals that differ by a factor of two. Here and below, Ω is a circular frequency, measured relative to the centre frequency ω_0, $B = (\omega_0/c)\int n_2 I(z)dz$, where I is the peak intensity [28]. The method was generalised to the case of an arbitrary ratio of B-integrals and an arbitrary dispersion of the medium and was successfully applied to reconstruct the parameters of pulses in the telecommunication range using a two-centimetre piece of silica fibre as a nonlinear medium [30]. Below, we demonstrate the applicability of the method in a dispersion-free medium with only Kerr nonlinearity. The evolution of a pulse in such a medium can be described by the equation [35]

$$\frac{\partial E(t)}{\partial z} = i\gamma |E(t)|^2 E(t). \qquad (18)$$

The pulse field after passing through a nonlinear medium of length dz_j is related to the initial field by the expression

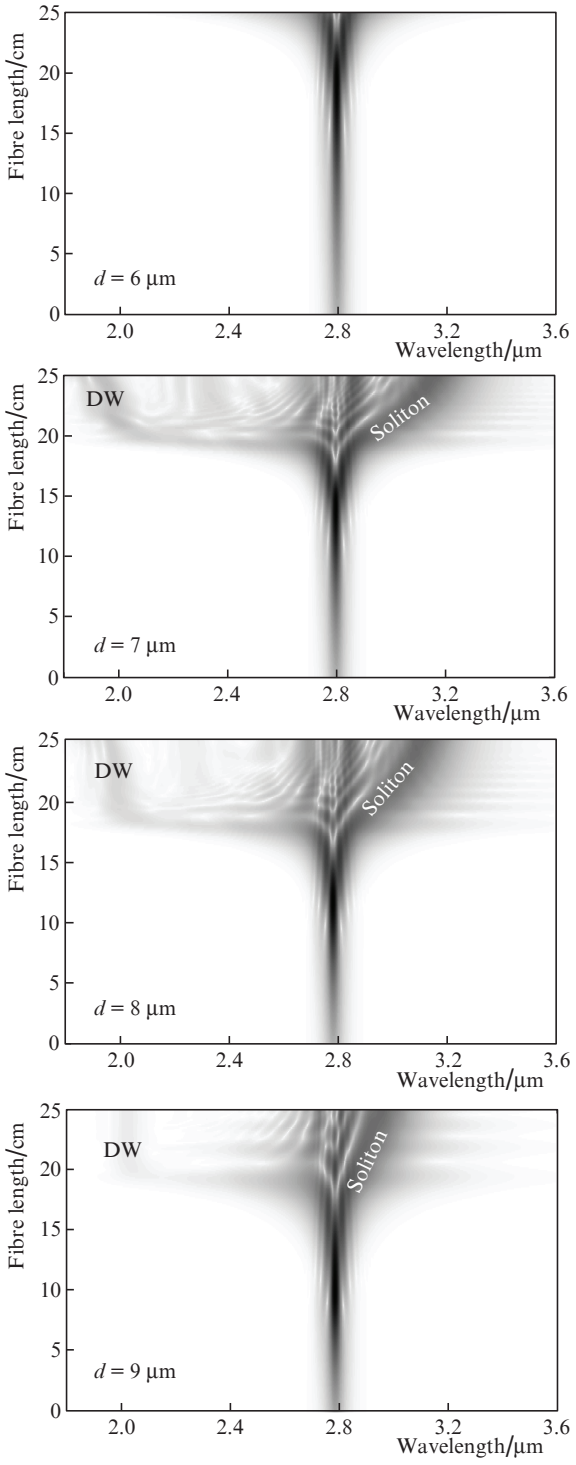

Figure 7. Spectral evolution of amplified pulses (function $|\tilde{E}(z,\lambda)|^{1/2}$) in fibres with different diameters d; (DW) dispersion waves.

$$E_j(t) = E_0(t)\exp[\mathrm{i}\gamma \mathrm{d}z_j|E_0(t)|^2]. \quad (19)$$

Hereinafter, the index $j = 0$ refers to the original signal, and $j = 1, 2$ to the converted signals. The numerical scheme for restoring the structure of the pulse field based on the Gerchberg–Saxton algorithm is shown in Fig. 8. Let the pulse envelope in the spectral representation be given as $\tilde{E}_j(\Omega) = |\tilde{E}_j(\Omega)|\exp(\mathrm{i}\varphi_j)$, where φ_j is the spectral phase. The purpose of the algorithm is to choose such a spectral phase φ_0 that minimises the error function:

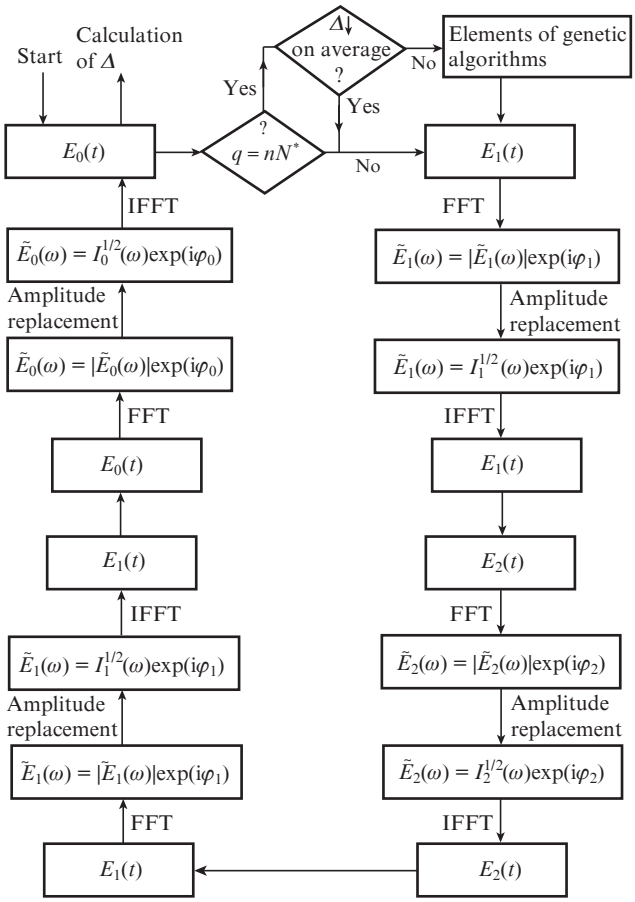

Figure 8. Flowchart of the algorithm for reconstructing the structure of the pulse field [q is the iteration number, n is a positive integer, and N^* = const (usually ~100)].

$$\Delta = \left\{\sum_{k=1}^{N}\left[I_1(\Omega_k) - |\tilde{E}_1(\Omega_k)|^2\right]^2 + \sum_{k=1}^{N}\left[I_2(\Omega_k) - |\tilde{E}_2(\Omega_k)|^2\right]^2\right\}, \quad (20)$$

where N is the number of points.

The algorithm is organised as follows (Fig. 8) [30]. First, an arbitrary signal is set and the field is calculated in accordance with Eqn. (19) in the time domain for a nonlinear medium having the length $\mathrm{d}z_1$. Next, the FFT is performed, then the spectral amplitude is replaced with the experimentally measured one, keeping the spectral phase unchanged, and finally the IFFT is performed. Then, the evolution in the time domain for a nonlinear medium of length $\mathrm{d}z_2$ is calculated, the FFT is performed, the spectral amplitude is replaced with the experimentally measured one and the IFFT is performed. Further, the backward propagation is calculated in the same way. As a result of the complete cycle, we obtain the new value $E_0(t)$. At the end of each qth iteration, the error function Δ is calculated using Eqn (20). If for a sufficiently large number of iterations the error does not decrease on average, then elements of genetic (crossover, mutation) algorithms are used. Note that for the operation of the algorithm, the exact values of B-integrals are not necessary, it is enough to know only their ratios [28]. A more detailed discussion of the algorithm, its limitations and area of applicability is beyond the scope of this paper. A detailed description of the related issues can be found in Ref. [30].

Let us consider the possibility of applying the described method to reconstructing the field structure of amplified

ultrashort signals directly in an erbium-doped tellurite glass optical fibre. In the absence of pumping or at low-intensity one, there is practically no stimulated absorption or amplification of pulses in the 2.7–3 μm wavelength range at the $^4I_{13/2} \rightarrow {}^4I_{11/2}$ transition, i.e., one can neglect the change in signal energy at lengths of a few centimetres or less. Suppose that the pumping is almost completely absorbed at a length shorter than the gain fibre length L, and we have registered the signal spectrum. Then we can cut a small piece dL_2 of the fibre (several millimetres long) and measure the spectrum, then cut off another piece of the fibre having the length dL_1 and measure the spectrum again. As a result of these manipulations, a fibre of length $L - dL_1 - dL_2$ will remain. Now we will consider the signal at the output of this doubly shortened fibre as an 'initial' signal. Two additional spectra at the output of the fibres of length $L - dL_2$ and L can be considered as the spectra of signals obtained as a result of the transformation of the 'initial' signal in nonlinear fibres with the lengths $dz_1 = dL_1$ and $dz_2 = dL_1 + dL_2$, respectively. Applying the developed algorithm to these three spectra, we reconstruct the intensity distribution and the phase of the pulse at the output of the remaining active fibre segment. The advantage of this approach is its extreme simplicity, due to the absence of any additional optical elements, as well as knowledge of the exact lengths of dz_1 and dz_2 and, accordingly, the ratio of B-integrals (since the energies in all cases are considered the same).

The applicability of the method is demonstrated in the following test example. Let us take a pulse with an energy of ~ 9 nJ and a duration of ~500 fs, obtained as a result of numerical simulation of the complete system of Eqns (9)–(17), with 15 cm length of active fibre and 7 μm diameter of core. The solid curves in Figs 9a and 9b show the pulse intensity in the time domain, as well as the spectral intensity and spectral phase. The spectra modelled for the complete system of equations for $dz_1 = 2.5$ mm, $dz_2 = 5$ mm (i.e. the total fibre lengths of 15.25 and 15.5 cm) are also shown in Figs 9c and 9d by solid curves. Next, we took only these three spectra and applied our algorithm to them in the dispersionless approximation, neglecting all the effects, except for the Kerr nonlinearity. By means of the computer program developed by us, the structure of the pulse field was reconstructed. The dashed curves in Fig. 9 display the solution found. Sufficiently good agreement between the original and reconstructed characteristics is seen. A minor discrepancy is due to the fact that the original spectra are obtained under the action of all linear and nonlinear effects in the optical fibre, while the restoration only takes into account the most fundamental effect of the Kerr nonlinearity.

7. Conclusions

We have theoretically shown for the first time the possibility of producing an amplifier of ultrashort optical pulses based on tellurite glass fibres doped with erbium ions in the 2.7–3 μm range at the transition $^4I_{11/2} \rightarrow {}^4I_{13/2}$. The numerical study has been carried out in the framework of a model comprising rate equations for level populations, an equation describing the evolution of the power of co-propagating pumping radiation at a wavelength of 0.975 μm, and the generalised nonlinear Schrödinger equation for the complex amplitude of the field of the amplified ultrashort pulse. The model takes into account the two-photon up-conversion process ($^4I_{13/2} + {}^4I_{13/2} \rightarrow {}^4I_{9/2} + {}^4I_{15/2}$), the absorption of light by

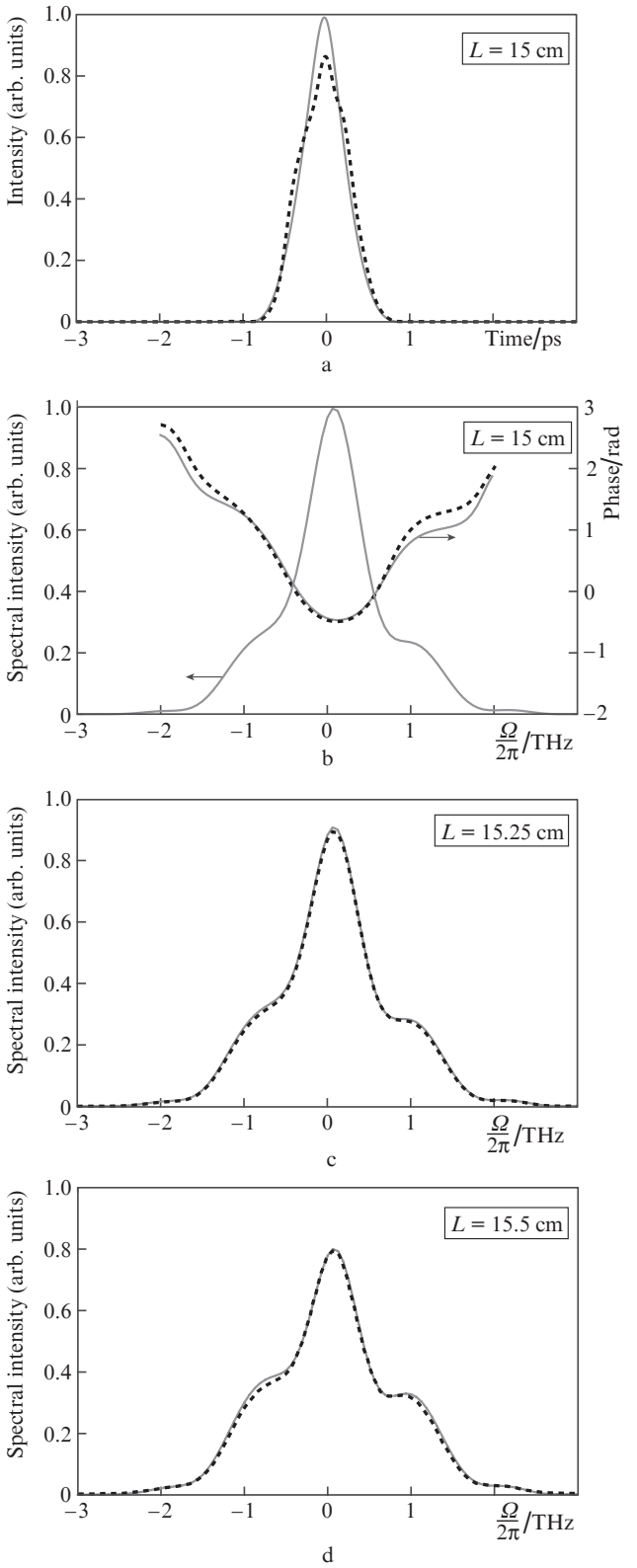

Figure 9. Reconstruction of the structure of a pulse field with an energy of ~9 nJ and a duration of ~500 fs, propagating in a fibre with a core diamter $d = 7$ μm: (a) intensity in the time domain for a fibre of length $L = 15$ cm, (b) spectral intensity and spectral phase at $L = 15$ cm, and (c, d) spectral intensities at L = (c) 15.25 and (d) 15.5 cm. The solid curves show the original structures obtained as a result of modelling the complete system of equations (9)–(17), and the dashed curves indicate the structures reconstructed as a result of the application of the algorithm. The frequency $\Omega/2\pi$ is measured starting from $\omega_0/2\pi$.

hydroxyl groups, and the multiphonon absorption, as well as fibre dispersion, linear losses, Kerr and Raman nonlinearities. Fibre optic samples have been fabricated based on high-purity $TeO_2-ZnO-La_2O_3-Na_2O$ glasses with a doped erbium core (ion concentration 10^{21} cm^{-3}) with a reduced content of hydroxyl groups, which ensures low absorption in the 2.7–3 μm range. The luminescence spectrum has been experimentally measured at the $^4I_{11/2} \rightarrow {}^4I_{13/2}$ transition, basing on which the emission cross section is calculated using the Füchtbauer–Ladenburg formula, and the absorption cross section is calculated using the McCumber method. The group velocity dispersions β_2, effective mode fields, nonlinear coefficients γ, and overlap integrals of the fundamental modes fields LP_{01} with the cross-section area Γ_{32} of the doped core for optical fibres with different core diameters has been determined by finding the eigenvalues and eigenfunctions of the Helmholtz equation. The measured and calculated parameters have been used in the numerical simulation of the spectral and temporal evolution of ultrashort pulses in the nonlinear active optical fibre.

The results of a series of numerical experiments show that a fibre with a core diameter of 7 μm and the following parameters at a wavelength of 2.8 μm are optimal for the amplifier: $\beta_2 = -150$ ps^2 km^{-1}, $\gamma = 7.5$ W^{-1} km^{-1}, $\Gamma_{32} = 0.5$. Such an active optical fibre allows generating pulses with ~10 nJ energy, 1 MHz repetition rate, less than 100 fs duration and ~20 dB amplification. Using a specially developed iterative computer algorithm based on the Gerchberg–Saxton algorithm, we have demonstrated that the intensity and phase of the generated pulses can be found by measuring their fundamental spectra and two additional spectra obtained by nonlinear optical conversion in short segments of the same active fibre without using additional optical elements.

Thus, the erbium ion-activated tellurite glass optical fibre seems to be a promising laser material for designing amplifiers for ultrashort pulses, as well as for measuring the structure of their field without using additional optical elements in the 2.7–3 μm range.

Acknowledgements. The manufacturing of tellurite glasses and optical fibres based on them, as well as the study of laser amplification, was carried out under the financial support from the Russian Science Foundation (Grant No. 17-12-01324). The study of the possibility of measuring the intensity and phase of ultrashort pulses was supported by the Russian Foundation for Basic Research and the Government of India, Department of Science and Technology (Grant No. 18-52-45005 IND_a). The development of a computer program for calculating the dispersion and mode fields was supported by the Ministry of Education and Science of the Russian Federation (Contract No. 14.W03.31.0032). The numerical simulation of the broadening of the spectrum and the compression of pulses was performed in the framework of the Extreme Light Fields and Their Interaction with Matter Programme of the Presidium of the Russian Academy of Sciences.

References

1. https://www.bccresearch.com/market-research/photonics/mid-infrared-lasers-technologies-applications-markets-report-pho016a.html.
2. Benson T.M., Furniss D., Tang Z., Sakr H., Seddon A.B., Sujecki S., in *Recent Trends in Computational Photonics.* Ed. by A. Agrawal, T. Benson, R.M. De La Rue, G.A.Wurtz (Springer, 2017) pp 39–75.
3. Aydın Y.O., Fortin V., Maes F., Jobin F., Jackson S.D., Vallée R., Bernier M. *Optica*, **4**, 235 (2017).
4. Mitrofanov A.V., Voronin A.A., Mitryukovskiy S.I., Sidorov-Biryukov D.A., Pugžlys A., Andriukaitis G., Flöry T., Stepanov E.A., Fedotov A.B., Baltuška A., Zheltikov A.M. *Opt. Lett*., **40**, 2068 (2015).
5. Sotor J., Martynkien T., Schunemann P.G., Mergo P., Rutkowski L., Soboń G. *Opt. Express*, **26**, 11756 (2018).
6. Gladyshev A.V., Kosolapov A.F., Khudyakov M.M., Yatsenko Yu.P., Kolyadin A.N., Krylov A.A., Pryamykov A.D., Biryukov A.S., Likhachev M.E., Bufetov I.A., Dianov E.M. *Quantum Electron*., **47**, 491 (2017) [*Kvantovaya Elektron*., **47**, 491 (2017)].
7. Kamynin V.A., Bednyakova A.E., Fedoruk M.P., Volkov I.A., Nishchev K.N., Kurkov A.S. *Laser Phys. Lett*., **12**, 065101 (2015).
8. Antipov O., Kolker D., Kal'yanov D., Larin S., Shur V., Akhmatkhanov A. *J. Opt. Soc. Am. B*, **35**, 1674 (2018).
9. Silaev A.A., Kostin V.A., Laryushin I.D., Vvedensky N.V. *JETP Lett*., **107**, 151 (2018) [*Pis'ma Zh. Eksp. Teor. Fiz*., **107**, 160 (2017)].
10. Anashkina E.A., Shiryaev V.S., Snopatin G.E., Muraviev S.V., Kim A.V. *J. Non-Cryst. Solids*, **480**, 38 (2018).
11. Karaksina E.V., Shiryaev V.S., Churbanov M.F., Anashkina E.A., Kotereva T.V., Snopatin G.E. *Opt. Mater*., **72**, 654 (2017).
12. Anashkina E.A., Andrianov A.V., Dorofeev V.V., Kim A.V. *Appl. Opt*., **55**, 4522 (2016).
13. Tao G., Ebendorff-Heidepriem H., Stolyarov A.M., Danto S., Badding J.V., Fink Y., Ballato J., Abouraddy A.F. *Adv. Opt. Photon*., **7**, 379 (2015).
14. Rivera V.A.G., Manzani D. *Technological Advances in Tellurite Glasses* (Springer International Publishing, 2017).
15. Lin A., Zhang A., Bushong E.J., Toulouse J. *Opt. Express*, **17**, 16716 (2009).
16. Yan X., Qin G., Liao M., Suzuki T., Ohishi Y. *J. Opt. Soc. Am. B*, **28**, 1831 (2011).
17. Gomes L., Oermann M., Ebendorff-Heidepriem H., Ottaway D., Monro T., Librantz A.F.H., Jackson S.D. *J. Appl. Phys*., **110**, 083111 (2011).
18. Ma Y., Guo Y., Huang F., Hu L., Zhang J. *J. Lumin*., **147**, 372 (2014).
19. Anashkina E.A., Dorofeev V.V., Koltashev V.V., Kim A.V. *Opt. Mater. Express*, **7**, 4337 (2017).
20. Smayev M.P., Dorofeev V.V., Moiseev A.N., Okhrimchuk A.G. *J. Non-Cryst. Solids*, **480**, 100 (2018).
21. Yakovlev A.I., Snetkov I.L., Dorofeev V.V., Motorin S.E. *J. Non-Cryst. Solids*, **480**, 90 (2018).
22. Churbanov M.F., Moiseev A.N., Chilyasov A.V., Dorofeev V.V., Kraev I.A., Lipatova M.M., Kotereva T.V., Dianov E.M., Plotnichenko V.G., Kryukova E.B. *J. Optoelectron. Adv. Mater*., **9**, 3229 (2007).
23. Moiseev A.N., Dorofeev V.V., Chilyasov A.V., Kut'in A.M., Pimenov V.G., Plotnichenko V.G., Koltashev V.V. *Inorg. Mater*., **43**, 675 (2007).
24. Moiseev A.N., Dorofeev V.V., Chilyasov A.V., Kraev I.A., Churbanov M.F., Kotereva T.V., Pimenov V.G., Snopatin G.E., Pushkin A.A., Gerasimenko V.V., Kosolapov A.F., Plotnichenko V.G., Dianov E.M. *Opt. Mater*., **33**, 1858 (2011).
25. Moiseev A.N., Dorofeev V.V., Chilyasov A.V., Pimenov V.G., Kotereva T.V., Kraev I.A., Ketkova L.A., Kosolapov A.F., Plotnichenko V.G., Koltashev V.V. *Inorg. Mater*., **47**, 665 (2011).
26. Anashkina E.A., Andrianov A.V., Koptev M.Yu., Muravyev S.V., Kim A.V. *Opt. Lett*., **39**, 2963 (2014).
27. Walmsley I.A., Dorrer C. *Adv. Opt. Photon*., **1**, 308 (2009).
28. Anashkina E.A., Ginzburg V.N., Kochetkov A.A., Yakovlev I.V., Kim A.V., Khazanov E.A. *Sci. Rep*., **6**, 33749 (2016).
29. Andrianov A.V., Kim A.V., Khazanov E.A. *Quantum Electron*., **47**, 236 (2017) [*Kvantovaya Elektron*., **47**, 236 (2017)].
30. Anashkina E.A., Andrianov A.V., Koptev M.Yu., Kim A.V. *IEEE J. Sel. Top. Quantum Electron*., **24**, 8700107 (2018).

31. Baudin K., Audo F., Finot C. *Microwave Opt. Technol. Lett*., **60**, 882 (2018).
32. Payne S.A., Chase L.L., Smith L.K., Kway W.L., Krupke W.F. *IEEE J. Quantum Electron*., **28**, 2619 (1992).
33. McCumber D. *Phys. Rev*., **136**, A299 (1964).
34. Snyder A.W., Love J. *Optical Waveguide Theory* (London–New York: Chapman and Hall, 1983).
35. Agrawal G.P. *Nonlinear Fiber Optics* (Academic Press, 2013).
36. Anashkina E.A., Kim A.V. *J. Lightwave Technol*., **35**, 5397 (2017).
37. Churkin D.V., Sugavanam S., Vatnik I.D., Wang Z., Podivilov E.V., Babin S.A., Rao Y., Turitsyn S.K. *Adv. Opt. Photon*., **7**, 516 (2015).
38. Nakazawa M., Kurokawa K., Kubota H., Suzuki K., Kimura Y. *Appl. Phys. Lett*., **57**, 653 (1990).
39. Balakin A.A., Litvak A.G., Mironov V.A., Skobelev S.A. *Quantum Electron*., **48**, 313 (2018) [*Kvantovaya Elektron*., **48**, 313 (2018)].
40. Kotov L.V., Koptev M.Yu., Anashkina E.A., Muravyev S.V., Andrianov A.V., Bubnov M.M., Ignat'ev A.D., Lipatov D.S., Gur'yanov A.N., Likhachev M.E., Kim A.V. *Quantum Electron*., **44**, 458 (2014) [*Kvantovaya Elektron*., **44**, 458 (2014)].